Inorg. Chem. **2006**, *45*, 2695–2703

Heteroleptic Cu(II) Dipyrromethene Complexes Linked via Hydrogen Bonds, Coordinative Bonds, and Covalent Bonds: Probing the Coordination Environment by Electron Paramagnetic Resonance Spectroscopy

Katja Heinze* and Anja Reinhart

Department of Inorganic Chemistry, University of Heidelberg, Im Neuenheimer Feld 270, 69120 Heidelberg, Germany

Received September 2, 2005

meso-Phenyldipyrromethene acetylacetonato copper(II) complexes [Cu(dpm-C_6H_4R)(acac)] (dpm-C_6H_4R = phenyl-substituted dipyrromethene, acac = acetylacetonato) with different substituents R at the phenyl moiety were synthesized. These substituents determine the mode of assembly into polymeric chains, namely, via hydrogen bonds, coordinative bonds, or covalent bonds (by immobilization on a polymer). Although the primary coordination sphere around the copper center is essentially identical for all complexes reported in this study (square-planar geometry with N_2O_2 coordination), subtle differences due to the different microenvironments have been observed in their structures, properties, and reactivity as probed by IR spectroscopy, electron paramagnetic resonance spectroscopy, magnetic measurements, thermal analyses, density functional theory calculations, and reaction with pyridine.

Introduction

There is currently an intense research effort to develop coordination polymers based on molecular precursors held together by forces of varying strength such as hydrogen bonds, coordinative bonds, and covalent bonds for magnetic and electronic materials as well as new classes of adsorbents, sensors, and storage materials.[1,2] The covalent immobilization of complexes on polymers has been used in heterogeneous catalysis,[3,4] chromatography,[5] and sensing applications[6,7] as well as in metal-complex-assisted solid-phase organic synthesis[8−14] and solid-phase synthesis of metal complexes.[15−19]

Self-complementary copper(II) complexes of meso-substituted pyridyl- and thioether-dipyrromethene (dpm) ligands have been employed by Cohen and co-workers to form coordination polymers and discrete oligomeric structures by linking the complexes through coordination bonds.[20−23] The use of different glues to assemble molecular complexes is expected to modify the properties of the

* To whom correspondence should be addressed. E-mail: katja.heinze@urz.uni-heidelberg.de. Tel.: (+49)6221-548471. Fax: (+49)-6221-545707.

(1) Kitagawa, S.; Kitaura, R.; Noro, S.-I. *Angew. Chem.* **2004**, *116*, 2388; *Angew. Chem., Int. Ed.* **2004**, *43*, 2334.
(2) Moulton, B.; Zaworotko, M. J. *Chem. Rev.* **2001**, *101*, 1629.
(3) *Chiral Catalyst Immobilization and Recycling*; De Vos, D. E., Vankelecom, I. F. J., Jacobs, P. A., Eds.; Wiley-VCH: Weinheim, Germany, 2000.
(4) Copéret, C.; Chabanas, M.; Saint-Arroman, R. P.; Basset, J.-M. *Angew. Chem.* **2003**, *115*, 164; *Angew. Chem., Int. Ed.* **2003**, *42*, 156.
(5) Shepherd, R. E. *Coord. Chem. Rev.* **2003**, *247*, 147.
(6) Albrecht, M.; Gossage, R. A.; Lutz, M.; Spek, A. L.; van Koten, G. *Chem.—Eur. J.* **2000**, *6*, 1431.
(7) Wu, D. G.; Ashkenasy, G.; Shvarts, D.; Ussyshkin, R. V.; Naaman, R.; Shanzer, A.; Cahen, D. *Angew. Chem.* **2000**, *112*, 4670; *Angew. Chem., Int. Ed.* **2000**, *39*, 4496.
(8) Comely, A. C.; Gibson, S. E.; Hales, N. J. *Chem. Commun.* **1999**, 2075.
(9) Gibson, S. E.; Hales, N. J.; Peplow, M. A. *Tetrahedron Lett.* **1999**, *40*, 1417.
(10) Bandoli, C.; Maiorana, S.; Licandro, E.; Casiraghi, L.; Zinzalla, G.; Senesi, P.; De Magistris, E.; Paio, A.; Marchioro, C. *J. Comb. Chem.* **2003**, *5*, 809.
(11) Mensi, N.; Isied, S. S. *J. Am. Chem. Soc.* **1987**, *109*, 7882.
(12) Arbo, B. E.; Isied, S. S. *Int. J. Pept. Protein Res.* **1993**, *42*, 138.
(13) Maiorana, S.; Seneci, P.; Rossi, T.; Baldoli, C.; Circao, M.; de Magistris, E.; Licandro, E.; Papagni, A.; Provera, S. *Tetrahedron Lett.* **1999**, *40*, 3635.
(14) Klapdohr, S.; Dötz, K. H.; Assenmacher, W.; Hoffbauer, W.; Hüsing, N.; Nieger, M.; Pfeiffer, J.; Popall, M.; Schubert, U.; Trimmel, G. *Chem.—Eur. J.* **2000**, *6*, 3006.
(15) Heinze, K.; Toro, J. B. *Eur. J. Inorg. Chem.* **2004**, 3498.
(16) Heinze, K.; Jacob, V.; Feige, C. *Eur. J. Inorg. Chem.* **2004**, 2053.
(17) Heinze, K.; Toro, J. B. *Angew. Chem.* **2003**, *115*, 4671; *Angew. Chem., Int. Ed.* **2003**, *42*, 4533.
(18) Heinze, K. *Chem.—Eur. J.* **2001**, *7*, 2922.
(19) Heinze, K.; Winterhalter, U.; Jannack, T. *Chem.—Eur. J.* **2000**, *6*, 4203.
(20) Halper, S. R.; Malachowski, M. R.; Delaney, H. M.; Cohen, S. M. *Inorg. Chem.* **2004**, *43*, 1242.

10.1021/ic0515047 CCC: $33.50 © 2006 American Chemical Society
Published on Web 02/25/2006

Scheme 1. Schematic Formation of Dipyrromethene Copper(II) Containing Polymers via (i) Hydrogen Bonds (X = $C_6H_4CONHiPr$), (ii) Coordinative Bonds (X = 3-Pyridyl, 4-Pyridyl, Quinolyl, $C_6H_4SCH_3$,[20−23] and $C_6H_4NO_2$), and (iii) Covalent Bonds (X = C_6H_4COO); L = Spectator Ligand; N∩N = Dipyrromethene Ligand

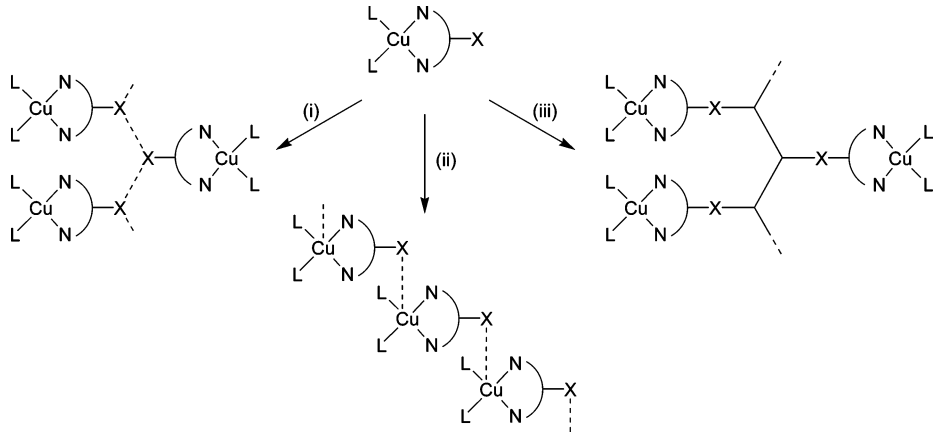

resulting materials, for example, magnetic behavior, stability, and reactivity.

Herein, we report on the assembly of dipyrromethene copper(II) complexes into polymers by comparatively weak hydrogen bonds and coordinative bonds via self-assembly processes as well as strong covalent bonds via immobilization on an insoluble polymer (Scheme 1). The influence of the different microenvironments on the coordination geometry, magnetic properties, stability, and reactivity of the dipyrromethene copper(II) complexes is probed by a variety of techniques.

Experimental Section

General Methods. Unless otherwise noted, the starting materials were obtained from commercial suppliers and used without further purification. The dipyrromethane precursors **1a**−**1d** were synthesized according to literature procedures.[24,25] IR spectra were recorded on a BioRad Excalibur FTS 3000 spectrometer using CsI disks. UV/vis spectra were recorded on a Perkin-Elmer Lambda 19, with 0.2 cm cells (Hellma, suprasil). Electron paramagnetic resonance (EPR) spectra were recorded with a Bruker ELEXSYS E500 spectrometer (X-band). Xsophe, version 1.0.2β was used for simulation of the spectra. Mass spectra were recorded on a Finnigan MAT 8400 spectrometer. Susceptibility measurements were performed on polycrystalline powders or dry polymers on a Quantum Design MPMS-XL-5 SQUID magnetometer in the temperature range 2−300 K with an applied field of 0.1 T in gelatin capsules. The diamagnetic contribution of the polymer was determined in a separate run. Differential scanning calorimetry (DSC) measurements were carried out on a Mettler DSC 30 under argon from 30 to 600 °C, at a heating rate of 10 K min^{-1}. Thermogravimetric measurements were carried out on a Mettler TC 15 under argon from 30 to 800 °C, at a heating rate of 10 K min^{-1}. Elemental analyses were performed by the microanalytical laboratory of the Organic Chemistry Department at the University of Heidelberg.

Computational Method. Density functional calculations were carried out with the Gaussian03/DFT (DFT = density functional theory) series of programs.[26] The B3LYP formulation of density functional theory was used employing the LANL2DZ or SDD basis sets for geometry optimizations (unrestricted, no symmetry constraints).[26] The structures of **2a**−**2c** and model compounds were characterized as minima by frequency analysis (N_{imag} = 0). Hyperfine coupling constants were obtained using the EPR-II basis set of Barone for H, C, N, and O, which is specifically optimized for the evaluation of hyperfine coupling constants.[27] For Cu, an all-electron basis set was used, namely, the 6-311G(d) basis set, because no optimized basis sets are available for transition metals.[28]

Complex Synthesis. The substituted dipyrromethane **1a**, **1b**, or **1c** (0.5 mmol) was dissolved in CH_2Cl_2 (20 mL). 2,3-Dichloro-5,6-dicyano-1,4-benzoquinone (DDQ; 114 mg, 0.5 mmol) was added, and the solution was stirred for 10 min. [$Cu(acac)_2$] (acac = acetylacetonato;198 mg, 0.75 mmol) was added as a solid, and the mixture was stirred for 12 h. The solution was evaporated to dryness, and the product was purified by column chromatography (SiO_2; 8:1 CH_2Cl_2/ethyl acetate) to afford dichroic red/green crystals.

2a. Yield: 20%. Anal. Calcd. for $C_{22}H_{20}N_2O_4Cu$: C, 60.06; H, 4.58; N, 6.37. Found: C, 60.75; H, 4.54; N, 6.74. EI-MS *m*/*z*: 439, [M^+]; 397, [$M - C_2H_2O]^+$; 340, [M − acac]$^+$. HR-EI *m*/*z*: 441.0727 [M^+, ^{65}Cu], 439.0744 [M^+, ^{63}Cu] (Calcd. *m*/*z*: 441.0715, 439.0819). UV/vis (CH_2Cl_2) λ_{max} (ϵ/L mol^{-1} cm^{-1}): 305 (19 600), 494 nm (32 900). IR (CsI) ν: 1724 (s, C═O_{ester}), 1582 (s, acac), 1555 (s, dpm), 1404 (s, dpm), 1381 (s, dpm), 1339 (s, dpm), 1281 (s, C−O), 1246 (s, dpm) cm^{-1}.

(21) Halper, S. R.; Cohen, S. M. *Angew. Chem.* **2004**, *116*, 2439; *Angew. Chem., Int. Ed.* **2004**, *43*, 2385.
(22) Halper, S. R.; Cohen, S. M. *Inorg. Chem.* **2005**, *44*, 4139.
(23) Do, L.; Halper, S. R.; Cohen, S. M. *Chem. Commun.* **2004**, 2662.
(24) Heinze, K.; Reinhart, A. *Z. Naturforsch., B: Chem. Sci.* **2005**, *60*, 758.
(25) Littler, B. J.; Miller, M. A.; Hung, C.-H.; Wagner, R. W.; O'Shea, D. F.; Boyle, P. D.; Lindsey, J. S. *J. Org. Chem.* **1999**, *64*, 1391.
(26) Frisch, M. J.; Trucks, G. W.; Schlegel, H. B.; Scuseria, G. E.; Robb, M. A.; Cheeseman, J. R.; Montgomery, J. A., Jr.; Vreven, T.; Kudin, K. N.; Burant, J. C.; Millam, J. M.; Iyengar, S. S.; Tomasi, J.; Barone, V.; Mennucci, B.; Cossi, M.; Scalmani, G.; Rega, N.; Petersson, G. A.; Nakatsuji, H.; Hada, M.; Ehara, M.; Toyota, K.; Fukuda, R.; Hasegawa, J.; Ishida, M.; Nakajima, T.; Honda, Y.; Kitao, O.; Nakai, H.; Klene, M.; Li, X.; Knox, J. E.; Hratchian, H. P.; Cross, J. B.; Bakken, V.; Adamo, C.; Jaramillo, J.; Gomperts, R.; Stratmann, R. E.; Yazyev, O.; Austin, A. J.; Cammi, R.; Pomelli, C.; Ochterski, J. W.; Ayala, P. Y.; Morokuma, K.; Voth, G. A.; Salvador, P.; Dannenberg, J. J.; Zakrzewski, V. G.; Dapprich, S.; Daniels, A. D.; Strain, M. C.; Farkas, O.; Malick, D. K.; Rabuck, A. D.; Raghavachari, K.; Foresman, J. B.; Ortiz, J. V.; Cui, Q.; Baboul, A. G.; Clifford, S.; Cioslowski, J.; Stefanov, B. B.; Liu, G.; Liashenko, A.; Piskorz, P.; Komaromi, I.; Martin, R. L.; Fox, D. J.; Keith, T.; Al-Laham, M. A.; Peng, C. Y.; Nanayakkara, A.; Challacombe, M.; Gill, P. M. W.; Johnson, B.; Chen, W.; Wong, M. W.; Gonzalez, C.; Pople, J. A. *Gaussian 03*, revision B.03; Gaussian, Inc.: Wallingford, CT, 2004.
(27) Barone, V. In *Recent Advances in Density Functional Methods*; Chong, D. P., Ed.; World Scientific Singapore: Singapore, 1995; Part 1.
(28) Munzarová, M.; Kaupp, M. *J. Phys. Chem. A.* **1999**, *103*, 9966.

2b. Yield: 23%. Anal. Calcd. for $C_{24}H_{25}N_3O_3Cu$: C, 61.72; H, 5.40; N, 9.00. Found: C, 60.90; H, 5.40; N, 8.60. EI-MS *m*/*z*: 466, $[M^+]$; 424, $[M - C_2H_2O]^+$; 367, $[M - acac]^+$. HR-EI *m*/*z*: 468.1199 [M^+, ^{65}Cu], 466.1255 [M^+, ^{63}Cu] (Calcd. *m*/*z*: 468.1190, 466.1292). UV/vis (CH_2Cl_2) λ_{max} (ϵ/L mol^{-1} cm^{-1}): 303 (19 400), 494 nm (30 400). IR (CsI) ν: 3264 (m, NH), 1628 (s, C═O_{amide}), 1585 (s, acac), 1562 (s, CN), 1547 (s, dpm), 1408 (s, dpm), 1377 (s, dpm), 1335 (s, dpm), 1261 (m), 1242 (s, dpm) cm^{-1}.

2c. Yield: 20%. Anal. Calcd. for $C_{20}H_{17}N_3O_4Cu$: C, 56.27; H, 4.01; N, 9.84. Found: C, 55.73; H, 3.98; N, 9.82. EI-MS *m*/*z*: 426, $[M^+]$; 327, $[M - acac]^+$. HR-EI *m*/*z*: 428.0514 [M^+, ^{65}Cu], 426.0518 [M^+, ^{63}Cu] (Calcd. *m*/*z:* 428.0510, 426.0615). UV/vis (CH_2Cl_2) λ_{max} (ϵ/L mol^{-1} cm^{-1}): 304 (20 100), 496 nm (29 600). IR (CsI) ν: 1593 (s, acac), 1554 (s, dpm), 1520 (s, NO_{asym}), 1404 (s, dpm), 1377 (s, dpm), 1350 (s, NO_{sym}), 1339 (s, dpm), 1246 (s, dpm) cm^{-1}.

1e. Wang resin (loading ca. 0.6−1.0 mmol g^{-1}; 500 mg; ca. 0.3−0.5 mmol) was suspended in CH_2Cl_2 (10 mL). **1d** (266 mg, 1.0 mmol) was dissolved in a minimum amount of N,N-dimethylformamide (DMF), and the solution was added to the resin. 4-(Dimethylamino)pyridine (DMAP; 6 mg, 0.05 mmol) and *N*,*N*′-diisopropylcarbodiimide (DIC; 128 mg, 1.0 mmol) were added, and the suspension was stirred for 16 h. Unreacted OH groups of the resin were protected by the addition of acetic anhydride (100 mg, 0.5 mmol) and pyridine (80 mg, 0.5 mmol) and stirring for 30 min. The resin was collected by filtration; washed with DMF (3×), CH_2Cl_2 (2×), ethanol (1×), and CH_2Cl_2 (3×); and dried in vacuo. IR (CsI) ν: 3417 (NH), 1720 (C═O_{ester}) cm^{-1}.

2d. 1e (500 mg, 0.3 mmol) was suspended in CH_2Cl_2 (30 mL). DDQ (228 mg, 1.0 mmol) was added, and the suspension was stirred for 10 min. [$Cu(acac)_2$] (396 mg, 1.5 mmol) was added, and the mixture was stirred for 12 h. The resin was collected by filtration, washed with DMF until the filtrate was colorless, and washed alternately with CH_2Cl_2 and ethanol (5×). After drying in vacuo, a green-reddish shining dark resin was obtained. IR (CsI) ν: 1721 (s, C═O_{ester}), 1407 (w, dpm), 1343 (w, dpm) cm^{-1}.

X-ray Crystallographic Analysis. The measurements were carried out on an Enraf-Nonius Kappa CCD diffractometer using graphite-monochromated Mo Kα radiation. The data were processed using the standard Nonius software.[29] All calculations were performed using the SHELXT PLUS software package. Structures were solved using direct or Patterson methods with the SHELXS-97 program and refined with the SHELXL-97 program.[30] Graphical handling of the structural data during refinement was performed using XMPA[31] and WinRay.[32] Atomic coordinates and anisotropic thermal parameters of the non-hydrogen atoms were refined by full-matrix least-squares calculations. Data relating to the structure determinations are collected in Table 1.

Results and Discussion

Synthesis of Heteroleptic Complexes. The dipyrromethanes **1a**−**1c** were synthesized according to literature procedures.[24,25] Oxidation of the dipyrromethanes to the corresponding dipyrromethenes was accomplished by DDQ. Subsequent reaction with a slight excess of [$Cu(acac)_2$] gave red solutions from which the heteroleptic complexes **2a**−**2c** (Scheme 2) were obtained by column chromatography.

Table 1. X-ray Data for **2a**, **2b**, and **2c**

	2a	**2b**[a]	**2c**
empirical formula	$C_{22}H_{20}N_2O_4Cu$	$C_{24}H_{24}N_3O_3Cu$	$C_{20}H_{17}N_3O_4Cu$
fw	439.94	466.00	426.91
space group	$P2_1/c$ (No.14)	Cc (No. 9)	$P2_1/c$ (No.14)
unit cell dimensions (Å, deg)	$a = 10.144(2)$ $b = 23.902(5)$ $c = 8.3310(17)$ $\alpha = 90$ $\beta = 105.81(3)$ $\gamma = 90$	$a = 9.4560(19)$ $b = 36.660(7)$ $c = 6.8970(14)$ $\alpha = 90$ $\beta = 114.51(3)$ $\gamma = 90$	$a = 13.917(3)$ $b = 8.9550(18)$ $c = 14.856(3)$ $\alpha = 90$ $\beta = 93.21(3)$ $\gamma = 90$
V (Å^3), Z	1943.5(7), 4	2175.5(8), 4	1848.5(6), 4
temp (K)	200	200	200
λ (Å)	0.710 73	0.710 73	0.710 73
D_{calcd} (mg m^{-3})	1.504	1.423	1.534
μ (mm^{-1})	1.156	1.035	1.214
final R indices [$I > 2\sigma(I)$][b]	$R_1 = 0.0413$ $wR_2 = 0.0931$	$R_1 = 0.0792$ $wR_2 = 0.1942$	$R_1 = 0.0665$ $wR_2 = 0.1531$
final R indices (all data)[b]	$R_1 = 0.0722$ $wR_2 = 0.1054$	$R_1 = 0.1343$ $wR_2 = 0.2390$	$R_1 = 0.1221$ $wR_2 = 0.1821$

[a] The crystal examined was a racemic twin with Flack $x = 0.48(3)$. [b] $R_1 = \sum|F_o - F_c|/|F_o|$. $R_2 = \{\sum[w(F_o^2 - F_c^2)^2]/\sum[wF_o^4]\}^{1/2}$.

Scheme 2. Synthesis of [Cu(dpm-C_6H_4R)(acac)] Complexes **2a**−**2c**; R = COOMe, CONH*i*Pr, and NO_2

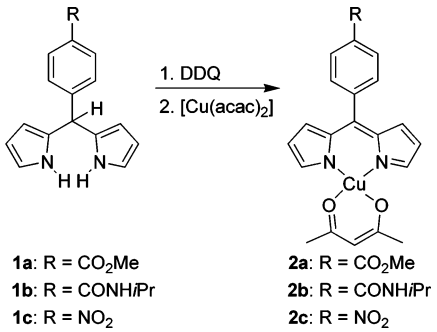

UV/vis and IR spectroscopy as well as mass spectrometry confirmed the formation of the desired heteroleptic complexes. In the UV/vis spectra, the characteristic charge-transfer bands[20] of heteroleptic [Cu(dpm)(acac)] complexes are observed at 494 nm, while the IR spectra show signals due to the dpm and acac ligands.[20] In addition, for **2a**, signals at 1724 and 1281 cm^{-1} characteristic for unperturbed ester groups are observed in the IR spectrum, while **2b** displays signals at 3264 cm^{-1} (amide A), 1628 cm^{-1} (amide I), and 1562 cm^{-1} (amide II) characteristic for hydrogen-bonded amide groups. Thus, the IR data of **2b** provide evidence for self-assembly of the complexes via hydrogen bonds (see below). The bands for the asymmetric and symmetric NO stretching vibrations of the nitro group present in **2c** are observed at 1520 and 1350 cm^{-1}. The EI mass spectra show signals for molecular ions with expected isotopic distribution, further confirming the successful synthesis of **2a**−**2c**.

The heteroleptic copper complexes are immobilized on a polymer by a two-step procedure (Scheme 3). The dipyrromethane ligand precursor **1d**[24] is attached to insoluble Wang resin (polystyrene-bound 4-benzyloxybenzyl alcohol; 0.6−1.0 mmol g^{-1}; 1% divinyl benzene) via esterification

(29) Hooft, R. *Collect*; Nonius: The Netherlands, 1998. http://www.nonius.com (accessed Feb 2006).
(30) (a) Sheldrick, G. M. *SHELXS-97*; University of Göttingen: Göttingen, Germany, 1997. Sheldrick, G. M. *SHELXL-97*; University of Göttingen: Göttingen, Germany, 1997. http://shelx.uni-ac.gwdg.de/SHELX/index.html (accessed Feb 2006). (b) *International Tables for X-ray Crystallography*; Kynoch Press: Birmingham, U.K., 1974; Vol. 4.
(31) Zsolnai, L.; Huttner, G. *XPMA*: University of Heidelberg: Heidelberg, Germany, 1998. http://www.rzuser.uni-heidelberg.de/~il1/laszlo/xpm.html (accessed Feb 2006).
(32) Soltek, R.; Huttner, G. *WinRay*; University of Heidelberg: Heidelberg, Germany, 1999. http://www.uni-heidelberg.de/institute/fak12/AC/huttner/frame/frame_soft.html (accessed Feb 2006).

Scheme 3. Immobilization of [Cu(dpm-C_6H_4R)(acac)] on Wang Resin

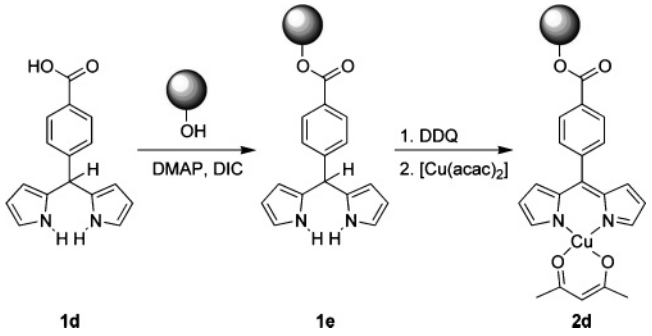

using DMAP and DIC as activators. This reaction is easily monitored by IR spectroscopy[19,33] because characteristic bands of the immobilized dipyrromethane appear at 3417 cm^{-1} (NH stretching vibration) and 1720 cm^{-1} (CO stretching vibration) in the IR spectrum of the washed and dried yellow polymer.

Notably, the signal of the NH stretching vibration of **1e** appears at a higher energy as compared to that of **1a**−**1d** (∼3350 cm^{-1}).[24] For **1a**−**1d**, intermolecular hydrogen bonds between the pyrrole NH groups and the substituent R have been observed in the solid state.[24,34] Obviously, this intermolecular interaction is suppressed by the polymer; that is, site isolation[35,36] of the dipyrromethanes seems to be operative under the conditions used (loading, cross-linking).

The immobilized dipyrromethane is oxidized by DDQ to the corresponding dipyrromethene and coordinated to the Cu(acac) fragment to give dark reddish-green **2d** analogously to the synthesis of the soluble complexes **2a**−**2c**.

The absence of bands for NH stretching vibrations in the IR spectrum of **2d** confirms the successful oxidation and complexation. The band for the CO stretching vibration of the ester remains unchanged as expected, while in the fingerprint region, new weak signals appear at 1407 and 1343 cm^{-1}, which can be assigned to dpm vibrations. All of the other characteristic bands of [Cu(dpm)(acac)] complexes are obscured by the signals of the polystyrene polymer.

Solid-State Structures of 2a−**2c.** Lustrous dichroic red/green crystals typical for complexes of dpm ligands were obtained from solutions of **2a**−**2c**. All of the complexes exhibit essentially square-planar geometry with Cu−N and Cu−O bond lengths of 1.96 and 1.93 Å, respectively, similar to other [Cu(dpm)(acac)] complexes (Table 2).[20−23] The aryl substituents are twisted out of plane with the dpm π system by 66°.

The ester-substituted complex **2a** crystallized as discrete complex molecules showing no short intermolecular contacts (Figure 1). As inferred from the IR data, the amide-substituted complex **2b** displays hydrogen bonding between the amide groups with N3···O1 = 2.85(1) Å (Figure 2), resulting in chains of molecules. In the crystal of **2c**, contacts between the copper ion and the nitro group of a neighboring molecule (O1···Cu1 = 2.96 Å[37]) furnish a square-pyramidal [4 + 1] coordination geometry of the copper center (Figure 3) similar to pyridyl and $C_6H_4SCH_3$ meso-substituted [Cu(dpm)(acac)] complexes.[20−23] The long O1···Cu1 distance is probably the result of "packing effects" in the crystal lattice rather than the formation of a strong copper−oxygen bond (no aggregation is observed in solution), but the intermolecular contact influences the properties of the solid material (see below). Thus, the nature of the remote substituent determines the mode of interaction in the solid state (no interaction, hydrogen bonds, or coordinative contacts).

Table 2. Selected Bond Lengths (Å) and Angles (deg) for **2a**−**2c**

	2a	**2b**	**2c**
Cu1−N1	1.951(2)	1.976(7)	1.963(4)
Cu1−N2	1.956(2)	1.952(8)	1.966(4)
Cu1−O2	1.9282(19)	1.929(6)	1.938(3)
Cu1−O3	1.9380(18)	1.924(7)	1.937(3)
N1−Cu1−N2	91.57(9)	90.6(3)	90.47(16)
N1−Cu1−O2	177.41(9)	176.1(3)	178.66(15)
N1−Cu1−O3	89.08(8)	91.3(3)	89.30(15)
N2−Cu1−O2	88.82(8)	87.7(3)	88.66(15)
N2−Cu1−O3	171.10(9)	176.5(3)	179.05(14)
O2−Cu1−O3	90.93(8)	90.6(3)	91.55(13)
C3−C4−C8−C9	−73.1(3)	−61(1)	−64.9(6)
Cu···Cu (shortest)	4.5	6.3	5.2
ω[a]	4.6	9.2	1.4

[a] Angle between CuO_2 and CuN_2 planes.

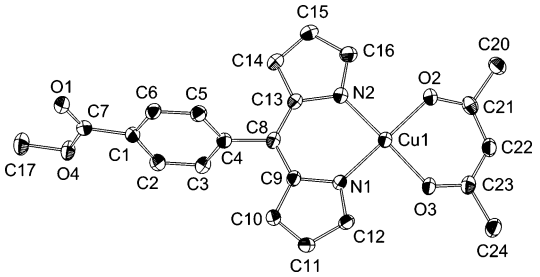

Figure 1. Structural diagram of **2a** with atom numbering scheme (hydrogen atoms omitted).

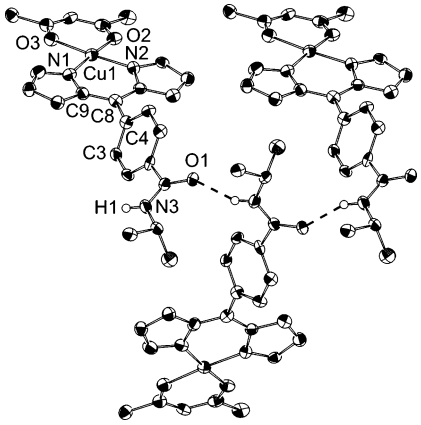

Figure 2. Structural diagram of **2b** with partial atom numbering scheme (hydrogen atoms omitted, except H1).

DFT Modeling of 2a−**2c.** The geometries of **2a**−**2c** and the parent complex [Cu(dpm)(acac)] were modeled by DFT

(33) Yan, B. *Acc. Chem. Res.* **1998**, *31*, 621.
(34) Patra, G. K.; Diskin-Posner, Y.; Goldberg, I. *Acta Crystallogr., Sect. E* **2002**, *58*, o530.
(35) Hodge, P. *Chem. Soc. Rev.* **1997**, *26*, 417.
(36) Scott, L. T.; Rebek, J.; Ovsyanko, L.; Sims, C. L. *J. Am. Chem. Soc.* **1977**, *99*, 625.
(37) For an example of Ar−NO_2 coordination to Cu(II), see: Kazak, C.; Yilmaz, V. T.; Yazicilar, T. K. *Acta Crystallogr., Sect. E* **2004**, *60*, m593.

Table 3. Selected Bond Lengths (Å) and Angles (deg) for **2a**, **2b**, and **2c** and the Model Complexes [Cu(dpm)(acac)] and [Cu(dpm)(acac)(py)] (B3LYP and LANL2DZ/SDD Basis Sets)

	2a	2b	2c	[Cu(dpm)(acac)][a]	[Cu(dpm)(acac)(py)][a]
Cu1−N1	1.970/1.960	1.970/1.959	1.972/1.962	1.967	1.992
Cu1−N2	1.970/1.960	1.970/1.959	1.972/1.962	1.967	1.990
Cu1−O2	1.981/1.970	1.982/1.970	1.979/1.967	1.969	2.004
Cu1−O3	1.980/1.970	1.982/1.970	1.979/1.967	1.969	2.006
N1−Cu1−N2	91.5/92.0	91.4/92.0	91.4/92.0	93.1	92.5
N1−Cu1−O2	178.2/177.8	178.0/177.6	178.4/178.1	177.7	167.7
N1−Cu1−O3	90.1/89.8	90.1/89.9	90.3/89.8	89.2	88.9
N2−Cu1−O2	90.1/89.8	90.1/89.9	90.0/89.8	89.2	88.6
N2−Cu1−O3	178.2/177.8	178.1/177.6	178.4/178.1	177.7	171.2
O2−Cu1−O3	88.4/88.3	88.3/88.3	88.5/88.5	88.5	88.2
C3−C4−C8−C9	−61.8/−62.1	−61.5/−61.7	−62.6/−62.8		
ω[b]	1.3/1.6	1.6/2.2	1.2/0.9	0.0	

[a] SDD basis set. [b] Angle between CuO_2 and CuN_2 planes.

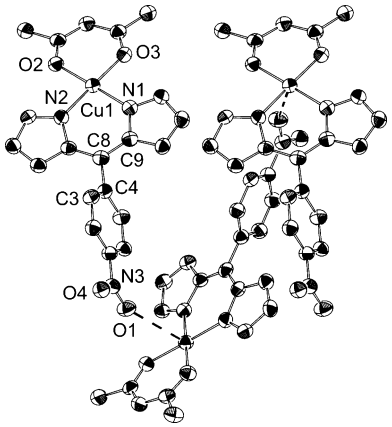

Figure 3. Structural diagram of **2c** with partial atom numbering scheme (hydrogen atoms omitted).

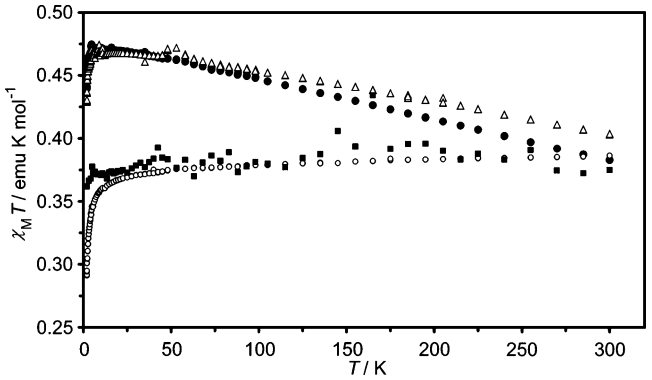

Figure 4. Variable-temperature magnetic data for **2a** (○), **2b** (△), **2c** (●), and **2d** (■).

calculations at the B3LYP level. The square-planar coordination environment (ω) and the torsion angle C3−C4−C8−C9 are well reproduced by the calculations. However, with the LANL2DZ basis set, the Cu−O and Cu−N bond lengths are overestimated by 0.05 and 0.01 Å, respectively (Tables 2 and 3). A better agreement with the experimental structures (Table 2) is obtained using the SDD pseudopotential (Table 3), so the SDD-derived geometry is used for further calculations (see below).

Magnetic Properties of 2a−2d. The temperature dependence of the product $\chi_M T$ of microcrystalline **2a**−**2d** has been measured at 0.1 T from 2 to 300 K (Figure 4, Table 4). Complexes **2a**−**2c** are paramagnetic with $\mu_{eff} = 1.76\,\mu_B$ ($\chi_M T = 0.383-0.403$ emu K mol^{-1}) at 300 K as expected for noninteracting $S = {}^1/_2$ systems.

Table 4. Magnetic and EPR[42] Data of **2a**−**2d**

	2a	2b	2c	2d[a]
μ_{eff} (300 K)/μ_B	1.76	1.79	1.75	1.70
C/emu K mol^{-1} [b]	0.385	0.421	0.409	0.385
θ/K[b]	−0.93	+2.37	+3.08	−0.04
g_{iso}	2.119	2.118	2.116	2.116
A_{iso}(Cu)/G	77	77	79	76
A_{iso}(N)/G	10	10	11	n.o.[c]
$g_{\|\|}$	2.230	2.230	2.230	2.226[c]
$A_{\|\|}$(Cu)/G	185	185	185	177[d]
$A_{\|\|}$(N)/G	11.6	11.6	n.o.[c]	n.o.[c]
$g_\perp$	2.05	2.05	2.05	2.05[d]
$A_\perp$(N)/G	15	15	15	14[d]

[a] Calculated for $M = 5000$ g mol^{-1} corresponding to a loading of 0.2 mmol g^{-1}. [b] Fitted using the Curie−Weiss law $\chi_M = C/(T - \theta)$ in the temperature range 2−300 K (see the Supporting Information). [c] n.o., not observed. [d] These measurements were performed at 300 K without adding solvent to the resin.

For **2a**, the product $\chi_M T$ remains constant down to ca. 50 K and drops to 0.291 emu K mol^{-1} at 2 K (Figure 4), indicative of weak antiferromagnetic interactions (Weiss constant $\theta = -0.93$ K), while for **2b** and **2c**, $\chi_M T$ increases to 0.47 emu K mol^{-1} at 4.6 K, indicative of weak ferromagnetic coupling ($\theta = +2.37$ K and +3.08 K, respectively). It is reasonable to ascribe the different magnetic behaviors to the different environments in the crystal structures.

In the crystal structure of **2a**, the complexes are stacked along the *c* axis with Cu···Cu distances of 4.5 Å (Table 2, Supporting Information), which could be the reason for the observed antiferromagnetic coupling (Scheme 4). For **2b** and **2c**, the Cu···Cu contacts are larger (Table 2) while these complexes are connected through hydrogen bonds and coordinative bonds, respectively, so that spin polarization along the dpm-C_6H_4R backbone could lead to the ferromagnetic coupling (Scheme 4).

The immobilized copper complex **2d**, however, behaves as an almost ideal paramagnet ($\theta = -0.04$ K; $\chi_M T = 0.362$ emu K mol^{-1} at 2 K). Thus, magnetic dilution of the spin carriers in the polymer is sufficient to prevent intermolecular magnetic interactions. This finding is also consistent with the absence of hydrogen-bonding interactions in the copper-free polymer **1e** (see above).

The loading of polymer **2d** was 0.18 mmol g^{-1}, determined by integrating the EPR signal of **2d** (see below) using a

Scheme 4. Possible Magnetic Interaction Pathways in **2a**−**2c**

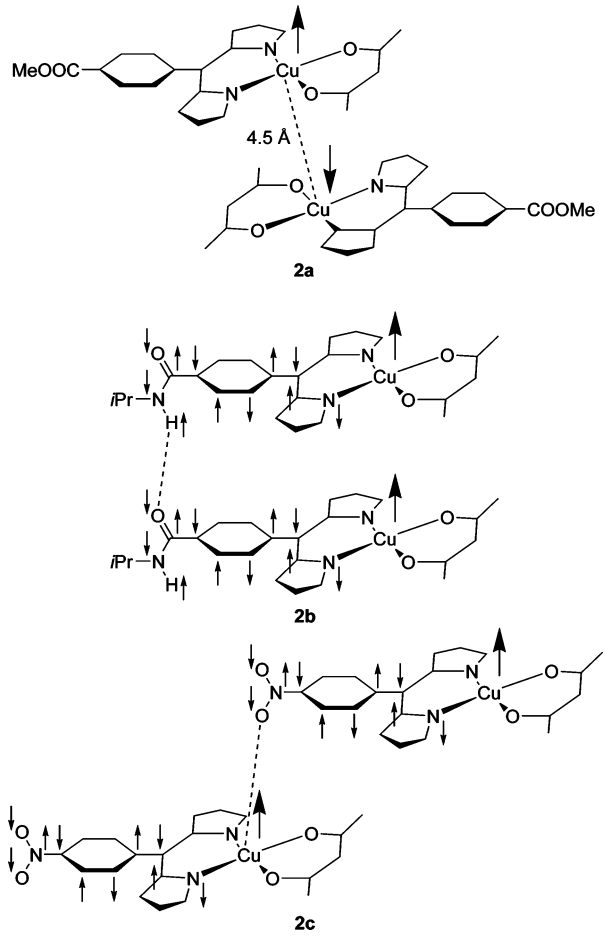

calibration curve of mechanically mixed polystyrene/divinyl benzene polymers and **2a** (Supporting Information). This value confirms the molecular mass estimated from magnetic measurements (5000 g mol^{-1}; 0.2 mmol g^{-1}). Thus, statistically, every complex unit in **2d** is surrounded by 45−50 styrene units of the polymer, accounting for the observed magnetic dilution.

EPR Spectroscopy of 2a−2d. The X-band EPR spectra of **2a**−**2c** were measured in solution at room temperature and in frozen solution at low temperature, while **2d** was investigated in the tetrahydrofuran (THF) gel phase at room temperature and low temperature and in the dry state at room temperature (Table 4). From the isotropic spectra, $g_{iso} \sim 2.117$, $A_{iso}(Cu) \sim 77$ G, and $A_{iso}(N) \sim 10$ G can be derived (Figure 5). The isotropic hyperfine coupling to the copper nucleus in **2a**−**2d** is significantly larger than that observed for bis(dipyrromethene) complexes [Cu(dpm)$_2$] [$A_{iso}(Cu) \sim 63$ G[38]]. This finding can be ascribed to the larger twisting of the ligand planes in homoleptic complexes ($\omega \sim 44°$ [39]) as compared to that of the square-planar heteroleptic complexes **2a**−**2d** with less steric congestion. Thus, the room-temperature EPR data confirm the square-planar geometry of the complexes in solution (**2a**−**2c**) and in the THF-swollen polymer (**2d**). In addition, the mobility of the immobilized copper complexes in the gel phase at room temperature is similar to that observed for **2a**−**2c** in a solution environment.[40,41]

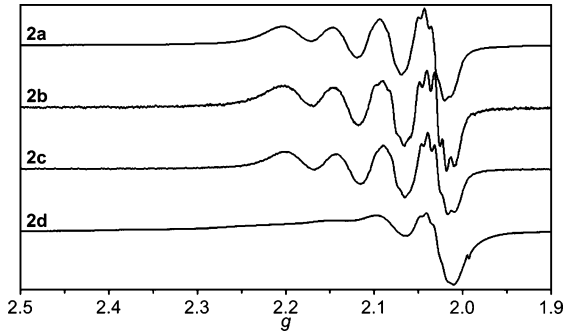

Figure 5. Isotropic X-band EPR spectra of **2a**−**2d** in THF at 300 K.

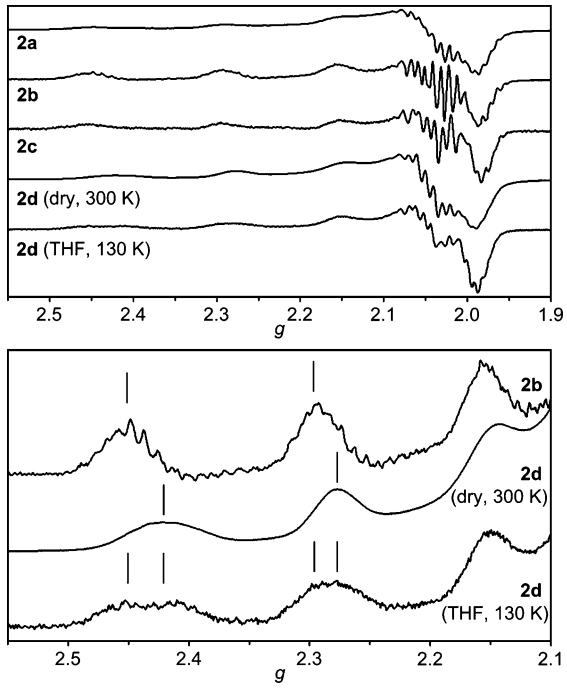

Figure 6. Top: anisotropic X-band EPR spectra of **2a**−**2c** (130 K, THF) and **2d** (300 K, solid; 130 K, THF). Bottom: expansion of the $g_{||}$ region for **2b** and **2d**.

The $A_{||}(Cu)$ values obtained from X-band EPR spectra in a frozen solution (Figure 6)[42] also reflect the difference in the coordination environment between square-planar **2a**−**2c** [$A_{||}(Cu) = 185$ G] and distorted homoleptic [Cu(dpm)$_2$] complexes [$A_{||}(Cu) < 165$ G[38]]. Similar observations have been reported for planar and saddled copper porphyrin complexes [$A_{||}$(Cu,planar) = 220 G; $A_{||}$(Cu,saddled) = 209 G].[43]

(38) Murakami, Y.; Matsuda, Y.; Sakata, K. *Inorg. Chem.* **1971**, *10*, 1734.
(39) Halper, S. R.; Cohen, S. M. *Chem.—Eur. J.* **2003**, *9*, 4661.
(40) Vaino, A. R.; Goodin, D. B.; Janda, K. D. *J. Comb. Chem.* **2000**, *2*, 330.
(41) Regen, S. L. *J. Am. Chem. Soc.* **1974**, *96*, 5275.
(42) The anisotropic EPR spectrum of **2b** has been simulated with Xsophe using the following parameters: natural isotope distribution $^{63/65}$Cu, $^{14/15}$N; *g*- and *A*-strain Gaussian line shape model; matrix diagonalization; 25 θ orientations; five field segments; orthorhombic symmetry; $g_x = 2.042$; $g_y = 2.054$; $g_z = 2.230$; $A_x(Cu) = A_y(Cu) = 25$ G; $A_z(Cu) = 185$ G; $A_x(N) = A_y(N) = 15$ G; $A_z(N) = 11.6$ G. In the text, g_x and g_y are expressed as $g_{||}$, g_z is expressed as $g_\perp$, A_x and A_y are expressed as $A_{||}$, and A_z is expressed as $A_\perp$ for convenience.
(43) Shao, J.; Steene, E.; Hoffman, B. M.; Ghosh, A. *Eur. J. Inorg. Chem.* **2005**, 1609.

Table 5. Selected Isotropic and Anisotropic Hyperfine Coupling Constants, Mulliken Spin Populations, Natural Atomic Charges, and Natural Electron Configurations of Selected Atoms Calculated for **2a**−**2c** Model Complex [Cu(dpm)(acac)] in Square-Planar and Distorted Geometries, and Model Complex [Cu(dpm)(acac)(py)]

	2a	**2b**	**2c**	[Cu(dpm)(acac)] (square-planar)	[Cu(dpm)(acac)] (mode a)[a]	[Cu(dpm)(acac)] (mode b)[b]	[Cu(dpm)(acac)(py)][c]
A_{iso}(Cu)/G	−122	−122	−122	−122	−113	−118	−108
A_{iso}(N)/G	17.1	17.1	17.0	16.7	14.6	17.4	15.8
$A_{\|\|}$(Cu)/G	−299	−299	−299	−299	−289	−290	−291
spin population Cu	0.6531	0.6530	0.6533	0.6549	0.6708	0.6403	0.6914
spin population N	0.0934	0.0937	0.0915	0.0918	0.0870	0.0943	0.0839
spin population O	0.0693	0.0690	0.0711	0.0704	0.0671	0.0747	0.0620
spin population C22	0.0006	0.0006	0.0007	0.0004	0.0082	0.0004	0.0005
natural charge on Cu	1.40	1.40	1.40	1.40	1.43	1.42	1.46
Cu natural electron configuration	$3d^{9.25}4s^{0.35}$	$3d^{9.25}4s^{0.35}$	$3d^{9.25}4s^{0.35}$	$3d^{9.25}4s^{0.35}4p^{0}$	$3d^{9.23}4s^{0.33}4p^{0.01}$	$3d^{9.26}4s^{0.32}4p^{0}$	$3d^{9.22}4s^{0.31}4p^{0.01}$
4s contribution/%	3.7	3.7	3.7	3.7	3.5	3.3	3.3

[a] $\omega = 40°$ (saddling, mode a). [b] C8−Cu1−C22, 130° (doming, mode b). [c] C8−Cu1−C22, 169°; Cu1−N_{py}, 2.342 Å.

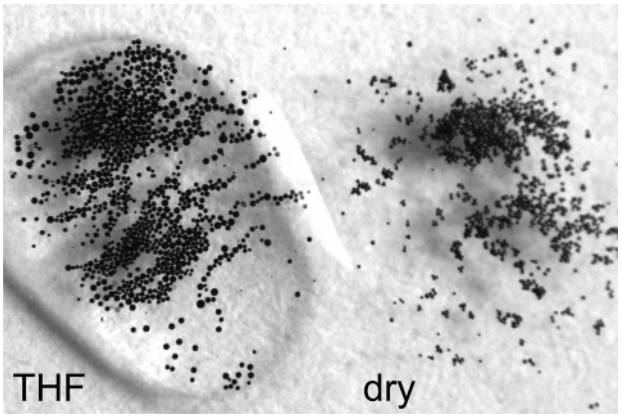

Figure 7. Photograph of THF-swollen and dry **2d**.

Scheme 5. Schematic Drawing of Nonplanar Distortions of [Cu(dpm)(acac)] Complexes: Saddling (mode a) and Doming (mode b)

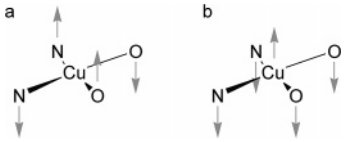

However, hyperfine coupling to the copper nucleus in dry **2d** $A_{||}$(Cu) = 177 G is significantly (96%) smaller than that observed for **2a**−**2c** (Figure 6, Table 4). This reduction of $A_{||}$(Cu) could be due to a distortion of the complexes in the dry polymer. Drying of the THF-swollen polymer results in shrinking of the polymer to approximately 60−65% of the original volume (Figure 7).[15,18,44] Thus, the internal pressure of the dry polymer is larger than in a frozen glass, and steric interactions with adjacent polymer chains might induce some deformation of the complexes. At 130 K (frozen glass), signals of the THF-swollen polymer **2d** in the $g_{||}$ region are broader than those of the dry polymer **2d** (Figure 6, bottom), indicating the presence of both square-planar [$A_{||}$(Cu) = ∼ 185 G] and distorted complexes [$A_{||}$(Cu) ∼ 177 G].

Possible low-energy deformations (deduced from DFT frequency analyses of **2a**−**2c**; around 20 cm^{-1}) are the twisting of the ligand planes (Scheme 5, left; mode a; saddling) and the out-of-plane displacement of the copper center (Scheme 5, right; mode b; doming), which both could account for the reduction of $A_{||}$(Cu) in dry **2d**.

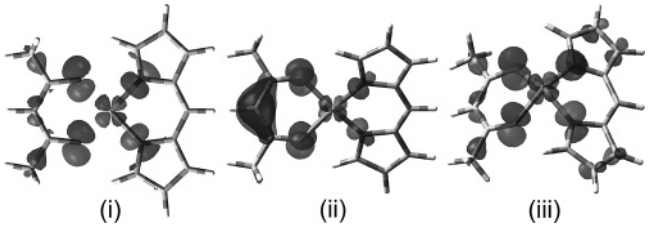

Figure 8. Singly occupied Kohn−Sham orbital of [Cu(dpm)(acac)] in square-planar (i) and distorted geometries; (ii) mode a ($\omega = 40°$); (iii) mode b (C8−Cu1−C22 = 130°) [isosurfaces at 0.05 au].

To substantiate the above assumptions, hyperfine coupling parameters were calculated by DFT methods for **2a**−**2c** and the model complex [Cu(dpm)(acac)] in square-planar and distorted geometries along modes a and b (Scheme 5, Supporting Information). For this purpose, the EPR-II basis set of Barone[27] for C, H, O, and N and an all-electron basis set 6-311G(d) for copper was employed in single-point calculations on the SDD-optimized geometry.

The calculated coupling constants are independent of the remote substituent R as observed experimentally (Tables 4 and 5). Coupling to dpm nitrogen nuclei is overestimated by about 170% and coupling to copper by about 160% (Tables 4 and 5).[45] The latter deviation is probably due to the 6-311G(d) basis set being used for copper because this basis set is not optimized for magnetic properties calculations and the employed B3LYP functional.[46]

Upon distortion from square-planar geometry along mode a or b, the isotropic and anisotropic coupling constants A_{iso}(Cu) and $A_{||}$(Cu) decrease as both distortions reduce the s character of the odd electron (Table 5, Supporting Information). In addition, spin density is delocalized onto the central carbon atom C22 of the acac ligand (mode a) or onto the nitrogen and oxygen donor atoms of the ligands (mode b; Table 5), which is reflected in the shape of the corresponding singly occupied molecular orbitals (Figure 8). To achieve a 96% reduction in $A_{||}$(Cu), the ligands have to twist by 40°

(44) Santini, R.; Griffith, M. C.; Qi, M. *Tetrahedron Lett.* **1998**, *39*, 8951.

(45) For the bis(benzene)chromium radical cation $[(C_6H_6)_2Cr]^{\bullet+}$, hyperfine coupling to chromium has been calculated as too small (66% of experimental value) with a similar DFT setup: Perrier, A.; Gourier, D.; Joubert, L.; Adamo, C. *Phys. Chem. Chem. Phys.* **2003**, *5*, 1337.

(46) Szilagyi, R. K.; Metz, M.; Solomon, E. I. *J. Phys. Chem. A* **2002**, *106*, 2994.

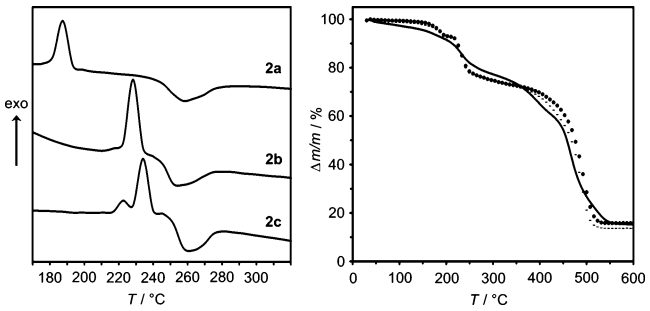

Figure 9. DSC plots and TGA curves of **2a**−**2c** (**2a**, full line; **2**, dashed line; **2c**, dotted line).

Table 6. Thermal Analyses Data of **2a**−**2c**

	2a	2b	2c
	TGA		
$\Delta m/m_{exp}$/% (T/°C)	5.9 (170)	6.4 (202)	7.0 (202)
$\Delta m/m_{calcd}$/% [X]	6.4 [CO]	6.0 [CO]	7.0 [NO]
$\Delta m/m_{exp}$/% (T/°C)	20.9 (350)	21.2 (350)	20.5 (350)
$\Delta m/m_{calcd}$/% [X]	22.5 [acac]	21.2 [acac]	23.2 [acac]
exptl. final weight/%	15.2	13.6	15.8
calcd. final weight/% [X]	14.4 [Cu]	13.6 [Cu]	14.9 [Cu]
	DSC		
T/°C (ΔH/kJ mol^{-1})	188 (−25.1)	228 (−51.1)	223 (−5.6)
T/°C (ΔH/kJ mol^{-1})			234 (−33.4)
T/°C (ΔH/kJ mol^{-1})	258 (40.4)	258 (49.3)	263 (44.2)

(saddling, mode a, halfway to a tetrahedron) or the ligands have to bend from 180° to 130° (doming, mode b, square-pyramid). Thus, both distortions may play a role for the complexes in the dry polymer **2d**.

Thermal Stability of 2a−2d. Thermal gravimetric analysis (TGA) was employed to evaluate the thermal stability of the copper(II) complexes **2a**−**2d** and their decomposition behavior with increasing temperature. The TGA plots of **2a**−**2c** show a three-step decomposition process (Figure 9, Table 6) with a sequential loss of a small molecule such as CO or NO ($\Delta m/m \sim 7\%$), the acac ligand ($\Delta m/m \sim 22\%$), and the dpm-C_6H_4R ligand ($\Delta m/m \sim 57\%$). Decomposition is complete at 550 °C, and the final weight percentage of $\Delta m/m \sim 14\%$ is in good agreement with that calculated for elemental copper (Table 6).

The DSC profiles of **2a**−**2c** show exothermic features at 188, 228, and 223/234 °C, respectively, which are associated with the liberation of a small molecule (Table 6). Thus, the thermal stability increases in the order **2a** < **2b** ∼ **2c**. An endothermic process tentatively assigned to melting and further decomposition (loss of the acac ligand; cf. mass spectrometric analyses; Experimental Section) is observed around 260 °C, which is in accordance with the observations made on [Cu(dpm)(acac)] complexes with pyridyl-substituted dpm ligands.[20]

For the immobilized complex **2d**, only the characteristic two-step decomposition of the polymer above 400 °C could be observed, very similar to that of the copper-free polymer **1d**.

Pyridine Uptake of 2a−2d. The square-planar complexes **2a**−**2d** were reacted with pyridine in a THF solution to form the pyridine adducts **2a**·py−**2d**·py.[47] In a THF solution, the adduct formation is fast, while it is very slow and incomplete when the dry solids are exposed to pyridine vapor.

The adducts are characterized by their EPR spectra in fluid and frozen solution. In all cases, **2a**·py−**2d**·py, the hyperfine coupling to copper is reduced as compared to the parent four-coordinate complexes **2a**−**2d** [**2a**·py−**2d**·py: $A_{iso}(Cu) = 70$ G[47] and $A_{||}(Cu) = 170$ G; Table 4]. The reduction of copper hyperfine coupling is due to the smaller s character of the odd electron in the pyridine adducts, which is well reproduced by a DFT calculation on the model complex [Cu(dpm)(acac)(py)] (Tables 3 and 5). The optimized geometry of the model complex matches the X-ray structures of [Cu(dpm-3-py)(acac)] and [Cu(dpm-4-py)(acac)],[20] with pyridine occupying the axial position of a square pyramid (observed: Cu1−N_{py} = 2.28 Å and 2.32 Å; calculated: Cu1−N_{py} = 2.34 Å; observed: C8−Cu1−C22 = 158° and 179°; calculated: C8−Cu1−C22 = 169°; for the numbering scheme, see Figure 1). For the model complex [Cu(dpm)(acac)(py)], $A_{iso}(Cu)$ is reduced to 88% and $A_{||}(Cu)$ to 97% as compared to that of [Cu(dpm)(acac)], which also reproduces the experimentally observed reductions to 91% and 92%, respectively. Pyridine coordination is reversible, and **2d** is especially easily recovered from **2d**·py by simply washing and filtering the insoluble polymer.

In summary, we have synthesized and characterized heteroleptic copper complexes with meso-substituted dipyrromethene ligands dpm-C_6H_4R. The substituent R determines whether the complexes remain monomeric in the solid state (**2a**, R = COOMe) or assemble to polymeric chains via hydrogen bonds (**2b**, R = CONH*i*Pr) or coordinative contacts (**2c**, R = NO_2). Immobilization has been achieved by attaching [Cu(dpm)(acac)] complexes to Wang resin (**2d**). Although the primary coordination sphere around the copper center is essentially identical for all of the complexes reported in this study (square-planar geometry with N_2O_2 coordination) subtle differences have been observed in their structures, properties, and reactivity.

Weak antiferromagnetic coupling is found for monomeric **2a**, while polymeric **2b** and **2c** are ferromagnetically coupled in the solid state. The polymer-bound complex **2d** behaves as an ideal paramagnet because of site isolation of the magnetic centers in the polymer. EPR spectroscopy in combination with DFT calculations [48] have been employed to study the coordination sphere of the copper center in different microenvironments because the hyperfine coupling to copper is very sensitive toward geometric changes (distortion and adduct formation). In the dry polymer **2d**, the complexes are distorted because of steric congestion and no pyridine adducts are formed. However, in the gel phase

(47) The amide-substituted complex **2b** does not form the pyridine adduct at room temperature in THF (1 equiv pyridine). Probably, the pyridine is hydrogen-bonded to the amide group in solution. In the frozen THF glass, however, pyridine coordinates to the copper center.

(48) For one example of combining DFT calculations and spectroscopy for "enzyme-immobilized" copper centers, see: DeBeer George, S.; Basumallick, L.; Szilagyi, R. K.; Randall, D. W.; Hill, M. G.; Nersissian, A. M.; Valentine, J. S.; Hedman, B.; Hodgson, K. O.; Solomon, E. I. *J. Am. Chem. Soc.* **2003**, *125*, 11314.

of **2d**, the immobilized complexes exhibit the stable square-planar geometry and are mobile enough to exhibit isotropic EPR spectra. In addition, the swollen polymer **2d** reacts easily and reversibly with pyridine to form immobilized square-pyramidal complexes.

Acknowledgment. This work was supported by the Deutsche Forschungsgemeinschaft, the Fonds der Chemischen Industrie, and the Dr. Otto Röhm Gedächtnisstiftung. The permanent generous support from Prof. Dr. G. Huttner is gratefully acknowledged. We thank Simone Leingang and Jens Nägele for preparative assistance.

Supporting Information Available: Plots of $\chi_{M-}{}^{1}$ versus T for **2a**−**2d**, view of the stacking of **2a** along the *c* axis; EPR calibration using mechanically mixed polystyrene/divinyl benzene and **2a**; EPR simulation of **2b**; plot of DFT-calculated $A_{||}$(Cu) versus angle between ligand planes ω for [Cu(dpm)(acac)]; plot of DFT-calculated $A_{||}$(Cu) versus angle C8−Cu1−C22 for [Cu(dpm)(acac)]; Cartesian coordinates of the DFT-calculated geometry (B3LYP/SDD) of **2a**, **2b**, **2c**, [Cu(dpm)(acac)], and [Cu(dpm)(acac)(py)]; and crystallographic data in CIF format. This material is available free of charge via the Internet at http://pubs.acs.org. X-ray crystallographic files in CIF format are available free of charge via the Internet at http://www.ccdc.cam.ac.uk. Refer to CCDC reference numbers 282430, 282431, and 282432.

IC0515047